Research Article | Vol. 28, No. 17 / 17 August 2020 / Optics Express 24981
Optics EXPRESS

Broadband control of the optical properties of semiconductors through site-controlled self-assembly of microcrystals

JACOPO PEDRINI,[1,*] PAOLO BIAGIONI,[2] ANDREA BALLABIO,[3] ANDREA BARZAGHI,[3] MAURA BONZI,[1] EMILIANO BONERA,[1] GIOVANNI ISELLA,[3] AND FABIO PEZZOLI[1]

[1]*L-NESS and Università degli Studi di Milano-Bicocca, Dipartimento di Scienza dei Materiali, via Cozzi, 55 - 20125, Milano, Italy*
[2]*Dipartimento di Fisica, Politecnico di Milano, Piazza Leonardo da Vinci, 32 –20133 Milano, Italy*
[3]*L-NESS and Politecnico di Milano, Via Anzani, 42 - 22100 Como, Italy*
[*]*jacopo.pedrini@unimib.it*

Abstract: We investigate light-matter interactions in periodic silicon microcrystals fabricated combining top-down and bottom-up strategies. The morphology of the microcrystals, their periodic arrangement, and their high refractive index allow the exploration of photonic effects in microstructured architectures. We observe a notable decrease in reflectivity above the silicon bandgap from the ultraviolet to the near-infrared. Finite-difference time-domain simulations show that this phenomenon is accompanied by a ~2-fold absorption enhancement with respect to a flat sample. Finally, we demonstrate that ordered silicon microstructures enable a fine tuning of the light absorption by changing experimentally accessible knobs as pattern and growth parameters. This work will facilitate the implementation of optoelectronic devices based on high-density microcrystals arrays with optimized light-matter interactions.

1. Introduction

The quest for the monolithic fabrication of photonic and optoelectronic devices based on group-IV semiconductors requires the development of reliable wafer-scale manufacturing processes that possibly allow for the combination of high-quality materials with the existing mainstream silicon technology. In this framework, the synergy of top-down and bottom-up techniques with current industrial-grade methods of material fabrication can yield interesting and promising approaches to tailor materials functionalities and performances. It has already been demonstrated [1] that the out-of-equilibrium deposition [2] on deeply patterned Si substrates allows for vertical homo and heteroepitaxy [1,3,4] of various materials including silicon, [4] germanium, [1,5–7] silicon carbide, [7,8] and III-V semiconductors like gallium nitride [9] and gallium arsenide. [10–12] The resulting structures are typically composed of micrometer-sized, deeply etched Si seeds, or "pillars", on top of which high-quality, faceted epitaxial microcrystals develop. Such microcrystals are self-aligned along the growth direction and isolated from the nearest neighbors by a vacuum gap as small as 50 nm. [4] It is therefore possible to control the entirety of the structure by tailoring the growth and fabrication parameters both in the top-down etching and in the bottom-up deposition processes. This allows tuning the lateral size of the pillars, their spacing, and the etching depth by lithographic design, while changes in deposition parameters yield different microcrystal thickness, shape, and morphologies. [1,13] The vertical growth process allows fabricating densely-packed, several micrometers thick semiconductor microcrystals. Moreover, it has been shown that the geometric constraints of the vertical growth and the control on the surface morphology of the microcrystal allow for the expulsion of threading dislocations. [1,5,14,15] The self-limiting lateral expansion drives threading dislocations towards the microcrystal side facets.

#398098 https://doi.org/10.1364/OE.398098
Journal © 2020 Received 19 May 2020; revised 18 Jul 2020; accepted 21 Jul 2020; published 10 Aug 2020

Optics EXPRESS

The lateral expulsion of threading dislocations results in microcrystals of remarkable quality, with a large fraction of the material with no extended defects. Application-wise, the large thickness of the crystal favors light absorption, while the near-unity filling factor [4] is significant for the maximization of the active area of a device. Finally, the possibility to obtain dislocation expulsion could be exploited for the fabrication of devices composed of microcrystals with large high-quality areas, few defect centers and low recombination-generation noise. [16] All of the aforementioned properties are exciting and promising for the fabrication of self-standing, isolated, vertically aligned matrices of devices including light emitters as LEDs and light absorbers as photovoltaic cells or photodetectors with broadband sensitivity from the visible to the near-infrared (NIR).

The great versatility of the vertically grown microcrystals makes available a finely tunable platform for the analysis of light-matter interaction effects, that are of great interest in light of possible applications to optoelectronic devices. The microstructures, being made of high refractive index materials such as silicon (n>3.5) [17] or germanium (n>3.9), [18] can lead to the emergence of optical phenomena such as Mie and Fabry-Perot resonances, [19–21] whispering gallery modes, [22] diffraction, and light trapping, [23–25] particularly in the spectral region where the incident wavelength is comparable to the microcrystal size. Amongst the several effects, antireflection and light trapping are crucial for maximizing photon absorption [26] in a wealth of applications ranging from high-sensitivity photodetectors to solar cells. These effects need to be quantified and light-matter interactions in these microsystems still need to be scrutinized. To this scope, given the relevant role played by geometrical factors in such system, it is extremely useful to have self-assembled structures that can be easily tailored by design.

Hence, we focus on the model system provided by a series of Si microcrystals monolithically grown by homoepitaxy on a patterned matrix of Si (001) pillars. Specifically, we observe a strong reflectivity reduction in the epitaxially grown microstructure with respect to a flat silicon film. Finite-difference time-domain (FDTD) simulations allow us to determine that the decrease in reflectivity is the consequence of an increase in light absorption in the microcrystal. Moreover, we show that the absorption spatial distribution can be tuned to maximize light interaction within a specific region of the microcrystal.

2. Methods

2.1. Sample preparation

Si microcrystals have been deposited on patterned substrates by low-energy plasma-enhanced chemical vapor deposition. All the microcrystals were grown under the same conditions on pillars having the same lateral dimensions (D) but different inter-pillar gap (G) (see Fig. 1(a)). Notably, the concomitant growth on unpatterned areas of the same wafer provides us with the flat reference, which enabled to discriminate between material-induced features and structural effects. Optical lithography and reactive ion etching have been used to etch 8 μm tall Si pillars within a p-type Si wafer (ρ =1-10 Ωcm). The square pillars, with lateral dimension D =2 μm, are separated by a gap G equal to 1, 2 or 4 μm for the three different samples analyzed in this work (see Fig. 1(b)-1(d). For each chip, the overall patterned area is 0.8×0.8 mm^2, much larger than the spot size used for the optical measurements. The deposition has been performed at 750 °C with a growth rate of 5 nm/s for a total thickness of 5 μm. During growth, Si microcrystals nucleate on each etched pillar. In the first stages of growth the microcrystals expand both laterally and vertically. As the growth proceeds, lateral expansion can lead to crystal merging, as observed for the G = 1 μm pattern (Fig. 1(b)), or decrease dramatically, due to mutual shadowing effects between neighboring crystals, resulting in the vertical growth of Si microcrystals separated by tens of nanometers gaps as in the case of G =2 μm (Fig. 1(c)). Even when the inter-pillar gap is large, as in the case of G =4 μm (Fig. 1(d)), the vertical growth is much faster than the lateral growth.

Optics EXPRESS

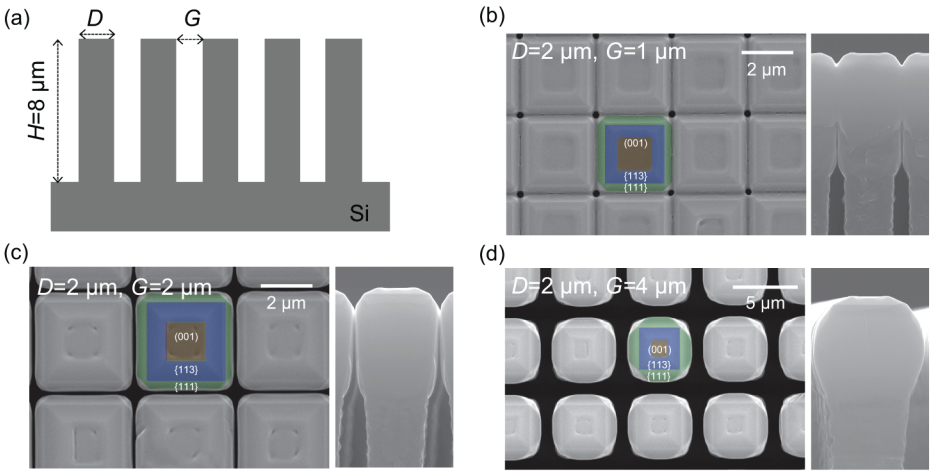

Fig. 1. a) Sketch of the etched pillar structure. b-d) Top view and side view scanning electron microscope (SEM) micrographs of the 5 µm Si microcrystals grown on a D =2 µm Si (001) seeds with G =1 µm (b), 2 µm (c), or 4 µm (d), respectively. The colored areas highlight the prominent facets of the microcrystals, i.e. the (001), {113}, and {111} (red, blue, and green, respectively).

2.2. Reflectivity measurements

The analysis of light interaction with the microstructured system was performed by measuring the diffuse reflectance, because specular reflectivity does not take into account diffusion and diffraction effects, that are clearly intense and noticeable even observing the sample by eye. Thus, reflectivity measurements were performed with a double-beam spectrophotometer using an integrating sphere to collect light over the full solid angle. The light sources were a tungsten iodine lamp for the spectral range between 0.3 and 2.5 µm and a deuterium arch lamp for the spectral range between 0.2 and 0.3 µm. The detectors were a photomultiplier tube for the visible and UV spectral range (coupled to a 1200 grid/mm grating), and a PbS photoconductive detector for the near-IR (coupled to a 300 grid/mm grating). The incident bandwidth was about 2 nm in the UV-Visible and 8 nm in the IR fraction of the spectrum. The scanning speed was 400 nm/min.

2.3. FDTD simulations

The numerical analysis relies on a commercial software implementing the FDTD method. [27] Due to the large size of the investigated structures compared to the wavelength, two-dimensional simulations have been performed, reproducing the cross section of each microstructure with proper periodic boundary conditions and plane-wave illumination. The frequency-dependent dielectric constant of Si is taken from the literature. [28] High-accuracy conformal meshing, as provided by the software, was employed for the discretization.

3. Results and discussion

Figure 1 reports scanning electron microscopy (SEM) images of the epitaxially grown microcrystals. SEM micrographs demonstrate that the microcrystals touch and merge only for the smallest G, while they are clearly well-separated when the gap is larger than 2 µm. In all cases the top of the crystals features (001), {113}, and {111} facets. The relative extension of the different facets changes from sample to sample. As the gap between adjacent pillars increases, the amount of adatoms deposited on the {111} and {113} facets and diffusing towards the (001) facets also increases, thus leading to a reduction of the (001) facet area as indeed observed in Fig. 1. [4] The

Optics EXPRESS

extension of the prominent families of facets was extracted from the top-down SEM micrographs reported in Fig. 1. Details on the process and the value of the facet area can be found in Table S1 in the Supplement 1. While epitaxy already leads to some advantages in reducing light reflection with respect to the etched pillars, particularly under normal incidence (see Fig. S1 in Supplement 1), our goal is to address the role of crystal morphology in tuning the optical properties. Indeed, we expect that the difference in the microcrystal top morphology could have an impact on the optical properties, because it might affect the way in which electromagnetic fields couple into the material, generating different light-matter interactions that can be tuned by properly choosing the pattern geometry and growth parameters.

As shown in Fig. 2(a), the patterning of the sample has a strong effect on the optical properties of the structure. The reflectivity of the microstructured samples is about 50% lower than their flat counterpart, i.e. the unpatterned region of the same wafer. The presence of the flat and patterned regions on the same chip guarantees that the material properties of both areas are the same. To retrieve the geometrical contributions from the intrinsic effects, we normalized the reflectivity of the microstructure R_m to that of the flat substrate R_f. To this end, we define the quantity $\frac{\Delta R}{R}$ as follows:

$$\frac{\Delta R}{R} = \frac{R_m - R_f}{R_f}. \tag{1}$$

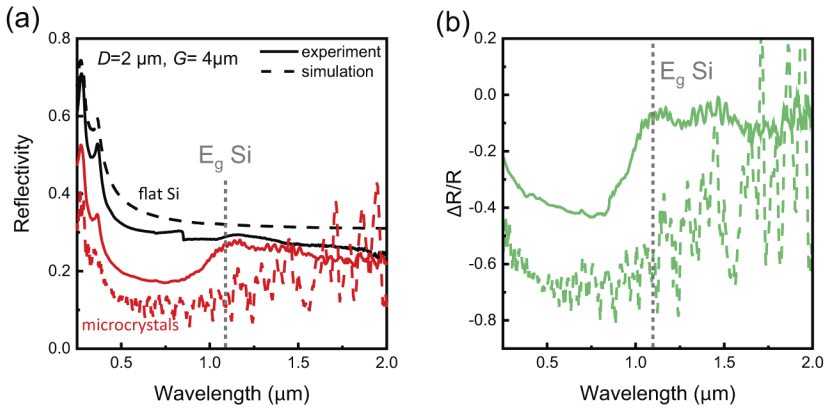

Fig. 2. a) Reflectivity spectra of a sample consisting of 5 μm Si microcrystals grown on Si (001) pillars with D =2 μm and G =4 μm. Solid lines are the experimental data collected on the flat surface (black) and the patterned area of the same sample (red). Dashed lines are the results of the two-dimensional FDTD simulations. b) Experimental (solid line) and simulated (dashed line) $\frac{\Delta R}{R} = \frac{R_m - R_f}{R_f}$ values.

$\frac{\Delta R}{R}$ is positive when the microstructured sample shows a larger reflectivity than the flat unprocessed area, and vice versa. As demonstrated in Fig. 2(b), it is possible to identify two distinct spectral regions. At short wavelengths $\frac{\Delta R}{R}$ has a pronounced dip that corresponds to a smaller reflectivity in the patterned structure than in the flat region. At long wavelengths, $\frac{\Delta R}{R}$ features clear oscillations superimposed to a negative plateau. The transition between the two regimes occurs around the silicon energy gap (~1.1 μm wavelength). This suggests that the decrease of reflectivity observed in the short-wavelength region is determined by the activation of the light absorption process. To gather insights into this phenomenon we performed two-dimensional FDTD simulations utilizing a realistic microcrystal shape. The comparison with the experimental data is reported in Fig. 2(a). FDTD simulations nicely reproduce the spectral position of the silicon peaks at 0.273 μm (4.5 eV) and 0.364 μm (3.4 eV) that are determined by the E_2 and by the experimentally non-resolved E_1 and E_0' interband transitions, respectively.

Optics EXPRESS

[29–31] The FDTD simulations also reproduce both the decrease in $\frac{\Delta R}{R}$ and the modulations observed experimentally. The difference in intensity of the modulations between the experiment and the simulation has to be ascribed to smoothing and averaging effect that are present in the fabricated structure, but not in the FDTD model. While the deviations in the absolute values of the calculated reflectivity from the experimental data are most likely to be ascribed to the 2D nature of the FDTD simulations, and to the simplified morphology of the simulated structure, these results demonstrate that the 2D FDTD calculation suffice to fully capture the origin of the optical response of our samples.

After showing that the patterned nature of the microcrystals introduces variations in the reflectivity with respect to the flat case, we investigate the impact of the pattern geometry. As reported in Fig. 3(a), we observe that the reflectivity of the microstructured samples can be tailored by changing the morphology of the microcrystals. We measured the diffuse reflectance of microcrystals grown on Si (001) pillars of the same lateral size (D = 2 μm) but with increasing inter-pillar gaps (G = 1, 2, and 4 μm, respectively). We observe that the decrease in $\frac{\Delta R}{R}$ in the transition from below to above bandgap is stronger for the samples with G =4 μm, and it is washed out when G is decreased to 1 μm. We can try to rationalize this behavior by considering that the side view SEM shown in Fig. 1(b) of the sample with G =1 μm shows significant merging between microcrystals. Indeed, also in the top-down SEM this sample looks like a continuous slab of silicon with narrow (<0.1 μm) gaps in a square lattice. Therefore the diffuse reflectivity of such a sample approaches that of the substrate. This is not the case for the other samples, where microcrystals are grown on more spaced pillars and thus the difference from the flat substrate is progressively marked, as shown in Fig. 1(c)-1(d). By analyzing $\frac{\Delta R}{R}$ as a function of the geometry of the patterned structure it is in principle possible to identify the conditions where the reflectivity is minimized, gathering useful information to design a device with engineered optical properties.

The origin of the observed reflectivity reduction above the bandgap can be possibly ascribed either to an increase of light absorption within the microcrystals or to a corresponding loss of light due to scattering and transmission through the substrate. To address this question we leverage FDTD modelling. Similarly to the quantity $\frac{\Delta R}{R}$, we define henceforth $\frac{\Delta A}{A}$ as the ratio of the differential absorption $\Delta A = A_m - A_f$ between the microcrystal and the reference to that absorbed by a flat reference A_f of the same thickness of the microcrystal. It is important to acknowledge that the microcrystal absorption A_m refers only to the 13 μm-thick patterned structure and does not take into account the substrate. For consistence, the absorption from the flat reference A_f is calculated in the superficial 13 μm-thick fraction of the flat, and not in the full, macroscopic wafer. This configuration was chosen in order to single out the contribution of just the microstructure composed of pillar and microcrystal, excluding the role of the substrate. The simulated $\frac{\Delta A}{A}$ curves are presented in Fig. 3(b). The relative increase in absorption between the patterned and unpatterned regions is remarkable. Indeed, it goes from ~0.1 at 1 μm up to ~1.6 in correspondence with the E_2 transition at 0.273 μm.

Fig. 3(a) and (b) allow us to gather additional insights. Indeed, while the reflectivity decreases by increasing the inter-pillar gap, the absorption does not demonstrate the same monotonic behavior, suggesting that additional mechanisms contribute to the reflectivity losses. It is unlikely for these losses to be caused by material defectivity. [32] Indeed, the quality of the material is guaranteed by their homoepitaxial nature. We ascribe the concomitant reduction in reflectivity and absorption when the interpillar distance approaches the largest value (4 μm) to the enhanced contribution of losses occurring through the substrate transmission. This phenomenon washes out the beneficial effect of patterning due to a less effective light trapping.

Notably, the FDTD modelling also allows us to single out the distribution of the light absorption occurring inside a single microcrystal. Since the intensity of the electromagnetic field is correlated to the absorption probability, we can localize the regions where absorption is maximized at any given wavelength. Indeed, the absorption density is proportional to the square modulus

Optics EXPRESS

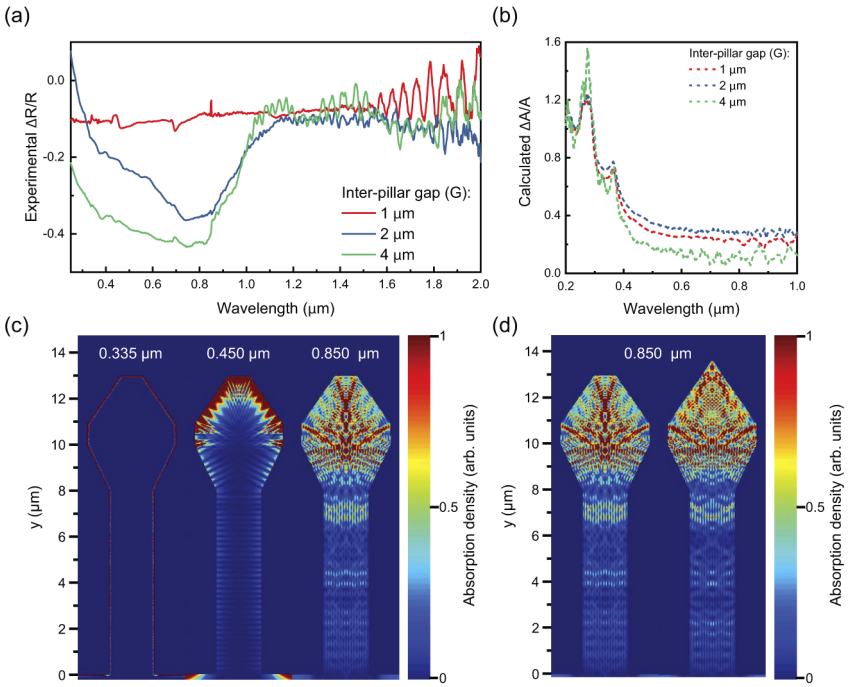

Fig. 3. (a) $\frac{\Delta R}{R} = \frac{R_m - R_f}{R_f}$ spectra for patterned samples composed of Si microcrystals grown on 2 × 2 μm^2 Si (001) pillars separated by 1 μm (red), 2 μm (blue), and 4 μm (green). (b) Simulated $\frac{\Delta A}{A} = \frac{A_m - A_f}{A_f}$ spectrum for the samples in (a). (c) Color coded map of the absorption density for a 5 μm thick microcrystal grown on a 8 μm pillar of D =2 μm and G =4 μm at a wavelength of 0.335 μm, 0.450 μm, and 0.850 μm. (d) Color coded map of the absorption density of the microcrystal described in (c) compared with one presenting a slightly different morphology, not showing the (001) facet.

of the electric field multiplied by the imaginary part of the dielectric constant of the material. Figure 3(c) reports the simulated absorption map of a single microcrystal mimicking the shape of crystals obtained for D =2 μm and G =4 μm.

As expected, at short wavelengths light is absorbed in the first superficial layers of the material, while at longer wavelengths it can penetrate deeper before being completely absorbed. The spatially resolved FDTD analysis allows us to understand the role of the surface in trapping the incident light inside of the microcrystal. This is particularly evident in the map at 0.850 μm. In this case, light can also be trapped by total internal reflection, and the multiple reflections from the surfaces determine an increase in absorption in the central region of the microcrystal. The FDTD modelling provides further insights on the experimental data. Since short-wavelength light is completely absorbed at the surface of the microcrystal, there is no sizeable difference between the three patterned samples regardless of their geometry. This is confirmed by the absorption capability of the patterned structures that is almost identical in the three reported samples. In the long wavelength regime, however, light can penetrate deeper into the microcrystal. It is thus trapped, experiencing multiple reflections at the sidewalls and generating an interference pattern that gives rise to the modulations observed at wavelengths above 0.6 μm in Fig. 3(b). It should be noted that the specific resonant modes associated with each investigated geometry possess however a low quality factor in this spectral range.

Optics EXPRESS

The FDTD modelling can also be employed as a guideline for the appropriate choice of design and fabrication parameters that affect the shape of the resulting microcrystals and their surface morphology. It is possible to perform an accurate analysis of the dependence of the absorption properties on the surface morphology. To this end, we compared the simulated absorption map of the structure reported in Fig. 3(c) with a similar structure, that differs only by the absence of the top (001) facet, as shown in Fig. 3(d). FDTD modelling shows that the light absorption distribution is clearly different in the two cases. In detail, the absorption density is more concentrated towards the center of the microcrystal in the structure that presents the (001) facet, while is more spread over the whole volume of the microcrystal when the (001) facet is removed. This difference in the absorption distribution between the two structures is appealing, because it shows that the morphology of the top surface can impact the propagation of the electromagnetic field in the microcrystal. This can result in structures where the incident light is focussed towards a specific region of the grown microcrystal. The morphologies simulated above can be obtained experimentally. Indeed, it has been demonstrated that the growth parameters can be tuned to fabricate microcrystals with the top (001) facet or, alternatively, with a pyramidal shape. [4,33] Therefore, the shape of the microcrystal can be determined *a priori*, paving the way for the fabrication of tailor-made microcrystals acting as a high-efficiency light harvester for a device where the active area is strategically placed in correspondence with the region of maximum absorption.

The analysis of the distribution of the electromagnetic field allows us to better understand also the origin of the modulations observed in the reflectivity data below bandgap. Figure 4(a) reports the details of the simulated reflectivity spectrum of a patterned area, having D =2 μm and G =4 μm, in the long-wavelength region. The reflectivity oscillates significantly between ~0.06 and ~0.4. Figure 4(b) reports the distribution of the absorption density calculated at the local minima (λ =1.243 μm, 1.567 μm) and maxima (λ =1.715 μm, 1.950 μm) of the spectrum reported in Fig. 4(a). There are two distinct effects that can be highlighted. First, the electromagnetic field is strongly confined in the microcrystals resembling a resonance or a cavity mode with high quality factor. In this case, light undergoes total internal reflection at the Si-air interface and the optical path that it experiences is greatly enhanced. In such a case, it is also possible to have a non-negligible absorption even below the Si energy gap, where the absorption coefficient is very small, but non-zero. [17] As confirmed by the absorption density, the simulation allows us to map with great clarity the distribution of the electric field in the microcrystal even below the Si

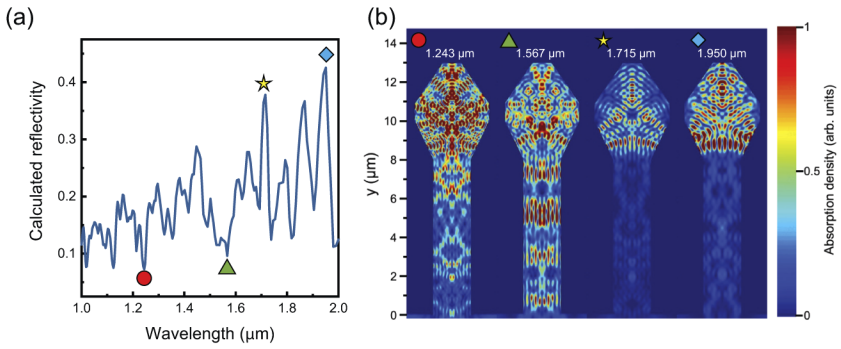

Fig. 4. (a) Simulated reflectivity spectrum of a 5 μm tall Si microcrystal grown on top of a 2 × 2 μm^2, 8 μm tall Si(001) pillar with 4 μm gap between neighboring pillars. The circle, triangle, star, and diamond mark the wavelengths at which the electromagnetic field is reported in panel b). (b) Color coded map of the absorption density of the microcrystal described in (a) at the wavelength of 1.243 μm, 1.567 μm, 1.715 μm, and 1.950 μm.

Optics EXPRESS

bandgap because the complex dielectric constant is non-zero, although very small. Moreover, in the etched pillar we can observe waveguided modes having different intensities. Specifically, at 1.715 μm and 1.950 μm the strength of the electromagnetic field inside the pillar is lower than at 1.243 μm and 1.567 μm, yielding a correlation between the calculated reflectivity and the intensity of the waveguided modes inside of the pillar. In detail, the reflectivity is higher when the waveguided light intensity is lower (i.e. at 1.715 μm and 1.950 μm), and vice versa. We therefore conclude that in this scenario, light experiences a lower reflection when a concomitant loss due to propagation in the substrate occurs. We can interpret the reflectivity modulations below the bandgap as critically dependent on the propagating modes in the fabricated pillars.

4. Conclusions and perspectives

In conclusion, we demonstrated that self-assembled silicon microcrystals vertically grown on deeply patterned Si substrates show a strong reflectivity decrease (up to 50%) with respect to a flat silicon sample. This reflectivity decrease is associated with an increase in light absorption efficiency inside the microstructures (up to ~2). The absorption properties can be tailored by design to match the desired applications, possibly increasing electrical power generation in a photovoltaic cell or detection effciency in a photodetector. Growth parameters provide suitable turning knobs to adjust light absorption and focussing towards specific areas of the microcrystals, offering larger tunability than in other approaches based on etched silicon nanowires [22,34] and localizing carrier generation away from the surfaces, possibly decreasing nonradiative recombination. While there are techniques that enable larger reflectivity decrease, such as those developed for photovoltaics applications, our flexible approach has several advantages with respect to conventional fabrication methods that do not exploit epitaxy. [35] The conclusions of this work can be naturally extended towards longer wavelengths by utilizing materials such as Ge. Moreover, vertical heteroepitaxy can be employed to fabricate complex epitaxial heterostructures with high quality, low defectivity, and optimized absorption, that are crucial in low-light intensity applications, such as LIDAR and single-photon detectors.

Funding

H2020 Future and Emerging Technologies (766955); Regione Lombardia (242092).

Acknowledgments

We thank Oliver Skibitzki from IHP-Frankfurt Oder for substrate patterning, Dario Narducci and Leo Miglio from the University of Milano-Bicocca for the use of the integrating sphere and the fruitful discussion.

Disclosures

The authors declare no conflicts of interest.

See Supplement 1 for supporting content.

References

1. C. V. Falub, H. Von Känel, F. Isa, R. Bergamaschini, A. Marzegalli, D. Chrastina, G. Isella, E. Müller, P. Niedermann, and L. Miglio, "Scaling hetero-epitaxy from layers to three-dimensional crystals," Science **335**(6074), 1330–1334 (2012).
2. C. Rosenblad, H. R. Deller, A. Dommann, T. Meyer, P. Schroeter, and H. von Känel, "Silicon epitaxy by low-energy plasma enhanced chemical vapor deposition," J. Vac. Sci. Technol., A **16**(5), 2785–2790 (1998).

Optics EXPRESS

3. C. V. Falub, T. Kreiliger, A. G. Taboada, F. Isa, D. Chrastina, G. Isella, E. Müller, M. Meduna, R. Bergamaschini, A. Marzegalli, E. Bonera, F. Pezzoli, L. Miglio, P. Niedermann, A. Neels, A. Pezous, R. Kaufmann, A. Dommann, and H. Von Känel, "Three dimensional heteroepitaxy: A new path for monolithically integrating mismatched materials with silicon," *Proc. Int. Semicond. Conf.*, CAS **1**, 45–50 (2012).
4. R. Bergamaschini, F. Isa, C. V. Falub, P. Niedermann, E. Müller, G. Isella, H. Von Känel, and L. Miglio, "Self-aligned Ge and SiGe three-dimensional epitaxy on dense Si pillar arrays," Surf. Sci. Rep. **68**(3-4), 390–417 (2013).
5. F. Pezzoli, F. Isa, G. Isella, C. V. Falub, T. Kreiliger, M. Salvalaglio, R. Bergamaschini, E. Grilli, M. Guzzi, H. Von Känel, and L. Miglio, "Ge crystals on Si show their light," Phys. Rev. Appl. **1**(4), 044005 (2014).
6. F. Pezzoli, A. Giorgioni, K. Gallacher, F. Isa, P. Biagioni, R. W. Millar, E. Gatti, E. Grilli, E. Bonera, G. Isella, D. J. Paul, and L. Miglio, "Disentangling nonradiative recombination processes in Ge micro-crystals on Si substrates," Appl. Phys. Lett. **108**(26), 262103 (2016).
7. H. Von Känel, F. Isa, C. V. Falub, E. J. Barthazy, E. Muller, D. Chrastina, G. Isella, T. Kreiliger, A. G. Taboada, M. Meduna, R. Kaufmann, A. Neels, A. Dommann, P. Niedermann, F. Mancarella, M. Mauceri, M. Puglisi, D. Crippa, F. La Via, R. Anzalone, N. Piluso, R. Bergamaschini, A. Marzegalli, and L. Miglio, "Three-dimensional epitaxial Si1-xGex, Ge and SiC crystals on deeply patterned Si substrates," ECS Trans. **64**(6), 631–648 (2014).
8. M. Masullo, R. Bergamaschini, M. Albani, T. Kreiliger, M. Mauceri, D. Crippa, F. La Via, F. Montalenti, H. von Känel, and L. Miglio, "Growth and coalescence of 3C-SiC on Si(111) micro-pillars by a phase-field approach," Materials **12**(19), 3223 (2019).
9. F. Isa, C. Chèze, M. Siekacz, C. Hauswald, J. Lähnemann, S. Fernández-Garrido, T. Kreiliger, M. Ramsteiner, Y. A. R. Dasilva, O. Brandt, G. Isella, R. Erni, R. Calarco, H. Riechert, and L. Miglio, "Integration of GaN crystals on micropatterned Si(001) substrates by plasma-assisted molecular beam epitaxy," Cryst. Growth Des. **15**(10), 4886–4892 (2015).
10. R. Bergamaschini, S. Bietti, A. Castellano, C. Frigeri, C. V. Falub, A. Scaccabarozzi, M. Bollani, H. Von Känel, L. Miglio, and S. Sanguinetti, "Kinetic growth mode of epitaxial GaAs on Si(001) micro-pillars," J. Appl. Phys. **120**(24), 245702 (2016).
11. S. Bietti, A. Scaccabarozzi, C. Frigeri, M. Bollani, E. Bonera, C. V. Falub, H. Von Känel, L. Miglio, and S. Sanguinetti, "Monolithic integration of optical grade GaAs on Si (001) substrates deeply patterned at a micron scale," Appl. Phys. Lett. **103**(26), 262106 (2013).
12. A. G. Taboada, M. Meduna, M. Salvalaglio, F. Isa, T. Kreiliger, C. V. Falub, E. Barthazy Meier, E. Müller, L. Miglio, G. Isella, and H. Von Känel, "GaAs/Ge crystals grown on Si substrates patterned down to the micron scale," J. Appl. Phys. **119**(5), 055301 (2016).
13. A. Barzaghi, S. Firoozabadi, M. Salvalaglio, R. Bergamaschini, A. Ballabio, A. Beyer, M. Albani, J. Valente, A. Voigt, D. J. Paul, L. Miglio, F. Montalenti, K. Volz, and G. Isella, "Self-Assembly of Nanovoids in Si Microcrystals Epitaxially Grown on Deeply Patterned Substrates," Cryst. Growth Des. **20**(5), 2914–2920 (2020).
14. F. Montalenti, F. Rovaris, R. Bergamaschini, L. Miglio, M. Salvalaglio, G. Isella, F. Isa, and H. V. Känel, "Dislocation-free SiGe/Si heterostructures," Crystals **8**(6), 257 (2018).
15. F. Isa, M. Salvalaglio, Y. A. R. Dasilva, M. Meduna, M. Barget, A. Jung, T. Kreiliger, G. Isella, R. Erni, F. Pezzoli, E. Bonera, P. Niedermann, P. Gröning, F. Montalenti, and H. Von Känel, "Highly mismatched, dislocation-free SiGe/Si heterostructures," Adv. Mater. **28**(5), 884–888 (2016).
16. S. R. Morrison, "1/f noise from levels in a linear or planar array. IV. The origin of the Hooge parameter," J. Appl. Phys. **72**(9), 4113–4117 (1992).
17. S. Schinke, C. Peest, P. C Schmidt, J. Brendel, R. Bothe, K. Vogt, M. R. Kröger, I. Winter, S. Schirmacher, and A. Lim, "Uncertainty analysis for the coefficient of band-to-band absorption of crystalline silicon," AIP Adv. **5**(6), 067168 (2015).
18. H. H. Li, "Refractive index of silicon and germanium and its wavelength and temperature derivatives," J. Phys. Chem. Ref. Data **9**(3), 561–658 (1980).
19. F. J. Bezares, J. P. Long, O. J. Glembocki, J. Guo, R. W. Rendell, R. Kasica, L. Shirey, J. C. Owrutsky, and J. D. Caldwell, "Mie resonance-enhanced light absorption in periodic silicon nanopillar arrays," Opt. Express **21**(23), 27587–27601 (2013).
20. J. Berzinš, S. Fasold, T. Pertsch, S. M. Bäumer, and F. Setzpfandt, "Submicrometer nanostructure-based RGB filters for CMOS image sensors," ACS Photonics **6**(4), 1018–1025 (2019).
21. M. Celebrano, M. Baselli, M. Bollani, J. Frigerio, A. Bahgat Shehata, A. Della Frera, A. Tosi, A. Farina, F. Pezzoli, J. Osmond, X. Wu, B. Hecht, R. Sordan, D. Chrastina, G. Isella, L. Duó, M. Finazzi, and P. Biagioni, "Emission engineering in germanium nanoresonators," ACS Photonics **2**(1), 53–59 (2015).
22. K. Kim, S. Yoon, M. Seo, S. Lee, H. Cho, M. Meyyappan, and C. K. Baek, "Whispering gallery modes enhance the near-infrared photoresponse of hourglass-shaped silicon nanowire photodiodes," Nat. Electron. **2**(12), 572–579 (2019).
23. J. Yang, F. Luo, T. S. Kao, X. Li, G. W. Ho, J. Teng, X. Luo, and M. Hong, "Design and fabrication of broadband ultralow reflectivity black Si surfaces by laser micro/nanoprocessing," Light: Sci. Appl. **3**(7), e185 (2014).
24. M. K. Hedayati and M. Elbahri, "Antireflective coatings: conventional stacking layers and ultrathin plasmonic metasurfaces, a mini-review," Materials **9**(6), 497 (2016).
25. T. L. Phan and W. J. Yu, "CVD-Grown Carbon Nanotube Branches on Black Silicon Stems for Ultrahigh Absorbance in Wide Wavelength Range," Sci. Rep. **10**(1), 3441 (2020).

Optics EXPRESS

26. K. Zang, X. Jiang, Y. Huo, X. Ding, M. Morea, X. Chen, C. Y. Lu, J. Ma, M. Zhou, Z. Xia, Z. Yu, T. I. Kamins, Q. Zhang, and J. S. Harris, "Silicon single-photon avalanche diodes with nano-structured light trapping," Nat. Commun. **8**(1), 628 (2017).
27. "Lumerical inc., fdtd solutions, release 2018b, canada,".
28. E. D. Palik, *Handbook of Optical Constants of Solids* (Academic Press, 1997).
29. M. Cardona, K. L. Shaklee, and F. H. Pollak, "Electroreflectance at a semiconductor electrolyte interface," Phys. Rev. Lett. **154**(3), 696–720 (1967).
30. A. Daunois and D. E. Aspnes, "Electroreflectance and ellipsometry of silicon from 3 to 6 eV," Phys. Rev. B **18**(4), 1824–1839 (1978).
31. G. E. Jellison and F. A. Modine, "Optical functions of silicon between 1.7 and 4.7 eV at elevated temperatures," Phys. Rev. B **27**(12), 7466–7472 (1983).
32. G. Kissinger, J. Vanhellemont, C. Claeys, and H. Richter, "Observation of stacking faults an prismatic punching systems in silicon by light scattering tomography," J. Cryst. Growth **158**(3), 191–196 (1996).
33. A. Marzegalli, F. Isa, H. Groiss, E. Müller, C. V. Falub, A. G. Taboada, P. Niedermann, G. Isella, F. Schäffler, F. Montalenti, H. Von Känel, and L. Miglio, "Unexpected dominance of vertical dislocations in high-misfit Ge/Si(001) films and their elimination by deep substrate patterning," Adv. Mater. **25**(32), 4408–4412 (2013).
34. M. Ko, S. H. Baek, B. Song, J. W. Kang, S. A. Kim, and C. H. Cho, "Periodically Diameter-Modulated Semiconductor Nanowires for Enhanced Optical Absorption," Adv. Mater. **28**(13), 2504–2510 (2016).
35. H. Savin, P. Repo, G. Von Gastrow, P. Ortega, E. Calle, M. Garín, and R. Alcubilla, "Black silicon solar cells with interdigitated back-contacts achieve 22.1% efficiency," Nat. Nanotechnol. **10**(7), 624–628 (2015).